Cancer Research

MYC Mediates Large Oncosome-Induced Fibroblast Reprogramming in Prostate Cancer

Valentina R. Minciacchi[1], Cristiana Spinelli[1], Mariana Reis-Sobreiro[1], Lorenzo Cavallini[1,2], Sungyong You[1], Mandana Zandian[1], Xiaohong Li[3], Rajeev Mishra[6,9], Paola Chiarugi[2], Rosalyn M. Adam[4,5], Edwin M. Posadas[6], Giuseppe Viglietto[7], Michael R. Freeman[1,4,6], Emanuele Cocucci[8], Neil A. Bhowmick[9], and Dolores Di Vizio[1,4,5]

Abstract

Communication between cancer cells and the tumor microenvironment results in the modulation of complex signaling networks that facilitate tumor progression. Here, we describe a new mechanism of intercellular communication originating from large oncosomes (LO), which are cancer cell–derived, atypically large (1–10 μm) extracellular vesicles (EV). We demonstrate that, in the context of prostate cancer, LO harbor sustained AKT1 kinase activity, nominating them as active signaling platforms. Active AKT1 was detected in circulating EV from the plasma of metastatic prostate cancer patients and was LO specific. LO internalization induced reprogramming of human normal prostate fibroblasts as reflected by high levels of α-SMA, IL6, and MMP9. In turn, LO-reprogrammed normal prostate fibroblasts stimulated endothelial tube formation *in vitro* and promoted tumor growth in mice. Activation of stromal MYC was critical for this reprogramming and for the sustained cellular responses elicited by LO, both *in vitro* and *in vivo* in an AKT1-dependent manner. Inhibition of LO internalization prevented activation of MYC and impaired the tumor-supporting properties of fibroblasts. Overall, our data show that prostate cancer–derived LO powerfully promote establishment of a tumor-supportive environment by inducing a novel reprogramming of the stroma. This mechanism offers potential alternative options for patient treatment. *Cancer Res; 77(9); 2306–17.* ©*2017 AACR.*

Introduction

During the development of prostate cancer, the host microenvironment co-evolves with the tumor in establishing a positive feedback loop that plays a key role in disease onset and progression (1, 2). Extracellular vesicles (EV) are membrane-enclosed particles that contribute to tumor progression by establishing a tumor-supportive environment. Exosomes (Exo) are nano-sized EVs that have been implicated in angiogenesis, tolerogenic immune response, fibroblast activation, and preparation of the metastatic niche (3–6).

Highly migratory prostate cancer cells exhibit a pattern of motility characterized by dynamic formation of nonapoptotic membrane blebs. Pinching off of these blebs results in the release of abnormally large EVs (1–10 μm), which are referred to as "large oncosomes" (LO; refs. 7, 8). LO formation and release is enhanced by loss of the cytoskeletal regulator diaphanous related formin-3 (DIAPH3), which induces a transition from a mesenchymal to a more rapid, invasive, and metastatic "amoeboid" phenotype (9). Increased LO shedding is also observed in association with enforced expression of a membrane-bound myristoylated form of the serine-threonine protein kinase AKT1 (MyrAKT1), which is constitutively active, in LNCaP cells (7, 10).

LO released from amoeboid cancer cells are abundant in tumor tissues and plasma of patients and mice with metastatic prostate cancer, and are not detected in benign samples (10–12). LO are also bioactive, as demonstrated by their capacity to degrade extracellular matrices *in vitro* (10). However, whether these vesicles play specific functional roles in the tumor microenvironment is completely unknown. LO harbor distinct protein cargo in comparison with Exo, suggesting that LO might activate specific molecular pathways (11).

Here, we focused on defining whether and how LO facilitate the propagation of oncogenic signaling originating from the tumor cells and affecting the stroma. We demonstrate that LO are the EV population that harbors functionally active AKT1 and that these particles can be internalized by stromal cells, even given their large size in comparison with Exo. Internalization seems to occur via phagocytosis and is necessary for the consequent biological and

[1]Division of Cancer Biology and Therapeutics, Departments of Surgery, Biomedical Sciences and Pathology and Laboratory Medicine, Samuel Oschin Comprehensive Cancer Institute, Cedars-Sinai Medical Center, Los Angeles, California. [2]Department of Experimental and Clinical Biomedical Sciences, University of Florence, Florence, Italy. [3]Van Andel Institute, Grand Rapids, Michigan. [4]The Urological Diseases Research Center, Boston Children's Hospital, Boston, Massachusetts. [5]Department of Surgery, Harvard Medical School, Boston, Massachusetts. [6]Urologic Oncology Program and Uro-Oncology Research Laboratories, Samuel Oschin Comprehensive Cancer Institute, Cedars-Sinai Medical Center, Los Angeles, California. [7]Department of Experimental and Clinical Medicine, University Magna Graecia, Catanzaro, Italy. [8]Division of Hematology, Department of Internal Medicine, The Ohio State University, Columbus, Ohio. [9]Department of Medicine, Cedars-Sinai Medical Center, Los Angeles, California.

Note: Supplementary data for this article are available at Cancer Research Online (http://cancerres.aacrjournals.org/).

Corresponding Author: Dolores Di Vizio, Cedars-Sinai Medical Center/Boston Children's Hospital, 8700 Beverly Blvd, Los Angeles, CA 90048. Phone: 310-423-7709; Fax: 310-423-5454; E-mail: dolores.divizio@cshs.org

doi: 10.1158/0008-5472.CAN-16-2942

functional effects. LO uptake induces a specific "reprogramming" of the fibroblasts that results in their increased ability to stimulate tube formation in endothelial cells and to promote tumor growth *in vivo*. Activation of the transcription factor (TF) MYC in the fibroblasts is necessary to sustain the effects elicited by LO *in vitro* and *in vivo*. Our study shows for the first time that LO are capable of activating specific functional pathways in the microenvironment. Inhibiting these pathways prevents the horizontal propagation of oncogenic signals *in vitro* and *in vivo*.

Materials and Methods

Cell culture and reagents

$LNCaP^{MyrAKT1}$ cells were obtained and cultured as previously described (13). WPMY-1, PC3, 22Rv1 cells, and human umbilical vein endothelial cells (HUVEC) were purchased from the ATCC and cultured as previously described (7, 10). The normal associated human prostatic fibroblasts (NAF) were generated from surgical explants of patients diagnosed with benign prostatic hyperplasia (14). All cell lines were authenticated by short tandem repeat profiling, *in vivo* growth, and histology, and they were negative mycoplasma upon periodical testing (Lonza). Primary wild-type mouse fibroblasts were expanded and transduced with a commercially available c-MYC lentiviral vector. A detailed description of the reagents can be found in the Supplementary Materials and Methods section.

Patient specimens

Human studies were approved by a Cedars-Sinai Medical Center Institutional Review Board protocol (n. 00030191), in compliance with the declaration of Helsinki. All subjects provided informed consent for blood donation to be used for research purposes. Patient samples were obtained from the Urologic Oncology Program and the Cedars-Sinai BioBank.

EV isolation

EVs were isolated from platelet-poor plasma specimens or cell culture supernatants (obtained after 24 hours in serum-free media) as previously described (11). For functional studies, the EVs were used at a working concentration of 20 μg/mL, unless otherwise specified. This dose corresponds to the use of LO from 30 donor prostate cancer cells to treat 1 recipient cell, a result that is indicative of high biological potency.

Immunoblot analysis

Samples were lysed with RIPA cell lysis buffer supplemented with Octyl β-D-glucopyranoside (OCG), protease, and phosphatase inhibitors. Note that 10 μg per lane were loaded, and samples were blotted for indicated antibodies.

Tunable resistive pulse sensing measurements

EV preparations were submitted to tunable resistive pulse sensing (TRPS) analysis using a qNano instrument (IZON Science) as described previously (15).

PKH26 staining

For LO uptake experiments, LO were fluorescently labeled using the lipophilic membrane dye PKH26. LO were incubated with the dye for 3 minutes at room temperature, and the reaction was blocked by BSA 1%. LO were then washed in 5 mL of PBS to remove any unbound dye, concentrated by filtration as previously described (12), and collected in PBS.

Flow cytometry

For LO uptake detection, target cells were incubated with PKH26-labeled LO (from $\sim 3.3 \times 10^6$ $LNCaP^{MyrAKT1}$ cells) for 1 hour at 37°C or at 4°C. Cells were washed several times, trypsinized to remove surface-associated LO, and then analyzed using a Becton Dickinson LSR II, or analyzed and sorted using a Becton Dickinson FACSAria III. In experiments with pharmacologic inhibitors, the indicated compounds were added simultaneously with PKH26-labeled LO. Data analysis was performed using FlowJo software (Treestar). Relative fluorescent intensity (RFI) was calculated as the ratio between the mean fluorescence intensity of the treated cells and control cells. Experiments were performed in triplicate.

Confocal microscopy

WPMY-1 cells, after internalization of PKH26-labeled LO or treated with vehicle control, were sorted and plated on coverslip, fixed, and permeabilized in 4% paraformaldehyde and then imaged by confocal microscopy. In select experiments, cells were incubated with a FITC-conjugated HA antibody. Images were acquired on a Leica TCS SP spectral confocal microscope with white light laser (10).

RNA interference

Cells were transfected with specific siRNA oligos to transiently inhibit expression of DNM2 or MYC. The oligos were diluted in Lipofectamine RNAiMAX (Thermo Fisher Scientific) at a final concentration of 40 nmol/L and 100 nmol/L for 72 hours (DNM2; ref. 16) or 24 hours (MYC), in accordance to the manufacturer's instruction. The cells, tested for silencing efficiency, were used in select experiments.

RNA extraction and qRT-PCR

RNA was extracted using the RNeasy Mini Kit and then quantified using NanoDrop2000 (Thermo Scientific). Five hundred nanogram of total RNA were retro-transcribed into complementary DNA (cDNA) using the iScript Kit. The primer sequences are listed in Supplementary Table S1. qRT-PCR was run on a ABI Prism 7900HT Sequence Detection System (Applied Biosystems). The relative levels of each mRNA were calculated using the ΔΔCt, and either GAPDH or β-actin levels were used for normalizing data.

Tube-branching assay

A total of 20,000 HUVEC cells/well were plated on Growth Factor Reduced Matrigel coated wells (96-well plate; ref. 17) with (1) SF DMEM in the presence or absence of LO and Exo, (2) Dynasore-OH (Dyn) (20 μmol/L) in SFM, with LO or full media (FM; EGM-2, 2% serum), and (3) conditioned media (CM) from NAF previously exposed to LO and Exo. To obtain the CM, NAF were washed 3 times and then cultured in fresh SFM for 24 hours after treatment with LO (6 hours in SFM). The CM was cleared of cell debris prior to being placed on endothelial cells. After 6 hours of incubation at 37°C, images were recorded with an inverted Leica microscope equipped with an Olympus camera. Results were quantified by measuring the number of tubes per field (at least 4 fields) by phase-contrast microscopy and Image J.

TF array

Nuclear extract of WPMY-1 treated with LO or vehicle was obtained with a Nuclear Extraction Kit (Thermo Fisher Scientific). Note that 10 μg of nuclear extracts were assayed for the activity of 16 TFs using a Stem Cell TF Activation Profiling Plate Array I (Signosis) following the manufacturer's instruction.

Luciferase reporter assay

To perform the luciferase reporter assay, the pBV-Luc wt MBS1-4 vector containing the MYC-regulated cyclin-dependent kinase 4 (CDK4) promoter element (18) or the pBV-Luc empty vector was transfected into primary NAF with the pRL-SV40 vector expressing renilla luciferase as internal control. Twenty-four hours after transfection, the media were changed, and the cells were exposed to LO or vehicle for 6 hours. In select experiments, cells were pretreated with either Dyn for 30 minutes or p-AKT1 inhibitor AZD5363 for 12 hours before LO treatment. In the case of Dyn, after treating the cells with LO +/– Dyn, they were cultured in fresh media for 6 hours before measuring MYC activity. The luciferase activity was determined with the Dual-Luciferase Reporter Assay System following the manufacturer's instructions. The relative luciferase activity was calculated as ratio of firefly versus renilla luciferase activity. At least three biological replicates were performed for each assay.

RNA sequencing

NAF were exposed to LO or vehicle for 6 hours prior to RNA extraction as described above. RNA concentration and quality were tested respectively with Nanodrop 8000 (Thermo Scientific) and 2100 Bioanalyzer (Agilent). One microgram of total RNA per sample was used for library construction with the Illumina TruSeq Stranded mRNA Library Prep Kit. Libraries were thus multiplexed and sequenced across 4 lanes of a NextSeq 500 platform (Illumina) using 75 single-end sequencing. On average, about 20 million reads were generated from each sample.

Data processing and master regulator analysis

Raw reads obtained from RNA sequencing (RNA-seq) were aligned to the custom human GRCh38 transcriptome reference (http://www.gencodegenes.org) using Bowtie (version 1.1.1; ref. 19) and RSEM (version 1.2.20; ref. 20) with default parameters. The data were filtered in low or unexpressed genes and ribosomal RNAs, normalized, and then subjected to differential expression analysis in limma-voom. Data files from the RNA-seq analysis were deposited in the gene expression omnibus data bank under the accession code GSE87563. Master regulator analysis (MRA) was performed as previously described, using TF-target interaction information collected from public databases (21).

Mouse studies

All mouse studies were performed in accordance to the institutional guidelines (animal protocol #5911). Animals were monitored for abnormal tissue growth and euthanized if excessive health deterioration was observed. Subrenal capsule grafting was done in C57BL/6 male mice as previously reported (22). Alternatively, tumor cells were recombined with or without fibroblasts (4:1) and injected subcutaneously athymic nude mice. Pretreatment with LO was performed at a concentration of 100 μg/mL. Dyn and the MYC-i (10058-F4) were used at a concentration of 20 μmol/L. Tumor size was measured twice a week and calculated as: $^1/_2$ x width^2 x length. Tumor tissues were either stained with hematoxylin and eosin or immunostained with Ki67 antibody using established protocols (23).

Immunoprecipitation

Protein lysates were incubated with IgG or HA antibodies (4°C for 2 hours) followed by overnight incubation (4°C) with protein G agarose beads. The immunoprecipitate was analyzed through gel electrophoresis and immunoblotting or used for the kinase activity assay.

Kinase activity assay

To analyze kinase activity, a nonradioactive AKT Kinase Assay Kit (Cell Signaling Technology) was used following the manufacturer's instruction. GSK3α/β phosphorylation was detected by using the phospho-GSK3α/β (Ser21/9) antibody.

Statistical analysis

Plots show an average of at least three independent biological replicate. Experimental groups were compared using a two-tailed, unpaired, Student *t* test.

Results

EV-bound AKT1 is selectively present in LO

A recent report identified AKT1 and other kinases in blood EVs from patients with different epithelial tumor types (24). Because AKT1 is frequently activated in patients with metastatic prostate cancer as a result of genomic aberrations in the PI3K pathway, and the above report did not separate large from small EVs, we analyzed the distribution of EV-bound AKT1 in LO and Exo. Immunoblotting for AKT1 phosphorylated on Ser473 (a marker of kinase activation) was performed in LO and Exo obtained from the plasma of patients ($n = 12$) with metastatic prostate cancer. We used a protocol based on differential centrifugation to separate LO from Exo, followed by flotation (upward displacement) to exclude proteins and other EV-attached molecules (Fig. 1A; ref. 11). We found that LO harbor p-AKT1^{Ser473} at significantly higher levels than Exo (Fig. 1B; Supplementary Fig. S1A), despite high similarities in the total protein amount in most of the samples (Supplementary Fig. S1B). To further characterize the active AKT1 content in EVs, we isolated LO and Exo from LNCaP^{MyrAKT1} cells. TRPS analysis identified particles with a diameter ranging from 1.5 to 6.0 μm, in the LO fraction, and from 80 to 180 nm, in the Exo fraction (Fig. 1C). High levels of p-AKT1^{Ser473} were readily detectable in LO, whereas they were significantly lower in Exo (Fig. 1D). p-AKT1^{Ser473} was also detected in LO from PC3 and 22Rv1 prostate cancer cells, which express the active protein endogenously (Fig. 1E). These results reveal that active AKT1 is primarily localized in LO, when compared with Exo, in both cell line–derived and patient plasma samples, suggesting that LO might serve as mobile platforms for active kinases, and that the enzyme travels in the circulation protected in EVs.

LO are internalized by heterologous cells

EV uptake typically represents an important step for intercellular communication. However, very little is currently known about the mechanisms that cells adopt to internalize EVs larger than Exo (25). We exposed immortalized WPMY-1 myofibroblasts to LO labeled with the fluorescent dye PKH26 and quantitatively analyzed LO uptake by flow cytometry. LO uptake by

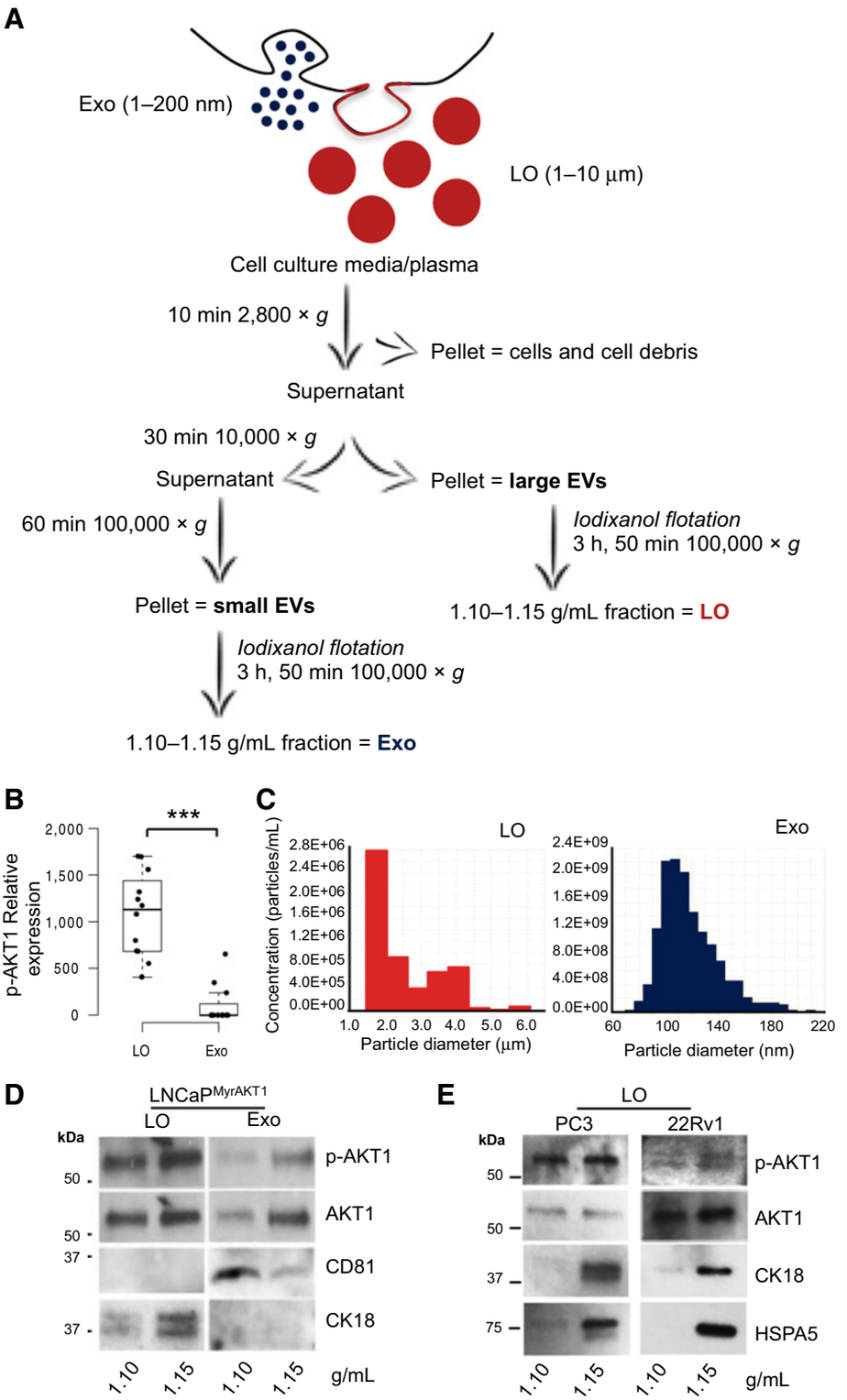

Figure 1.
LO are EVs that harbor active AKT1. **A,** Schematic representation of the protocol used for purification of LO and Exo starting from CM and patient plasma. **B,** Protein lysates from LO and Exo purified from the plasma (500 µL) of patients with castration-resistant prostate cancer ($n = 12$) were blotted with a p-AKT1^{Ser473} antibody. p-AKT1^{Ser473} band intensity was normalized to protein content for each patient. Circulating LO carry significantly higher levels of active AKT1 than Exo (***, $P < 0.002$). **C,** TRPS (qNano) analysis of LO (left) and Exo (right) using NP2000 and NP100 membrane pores, respectively. **D,** LO and Exo were purified from LNCaP^{MyrAKT1} cell media by gradient centrifugation (iodixanol), and protein lysates (10 µg) from the indicated fractions (1.10 and 1.15 g/mL density of the 10k and 100k pellets) were blotted with the indicated antibodies, including LO marker CK18 and Exo marker CD81. **E,** Equal amounts of protein from PC3- and 22Rv1-derived LO were blotted with the indicated antibodies.

target cells was quantitatively analyzed by flow cytometry (FACS; Fig. 2A). Confocal imaging of FACS-sorted LO-positive cells showed intact PKH26-labeled LO in the peripheral and perinuclear area (Fig. 2B). Increased PKH26 signal correlated with an increasing number of vesicles (Fig. 2C). In addition, we found colocalization of PKH26 with MyrAKT1 (Fig. 2D; Supplementary Fig. S2A), as detected with an HA-FITC antibody that binds with high specificity to the HA tag of the MyrAKT1 construct (10),

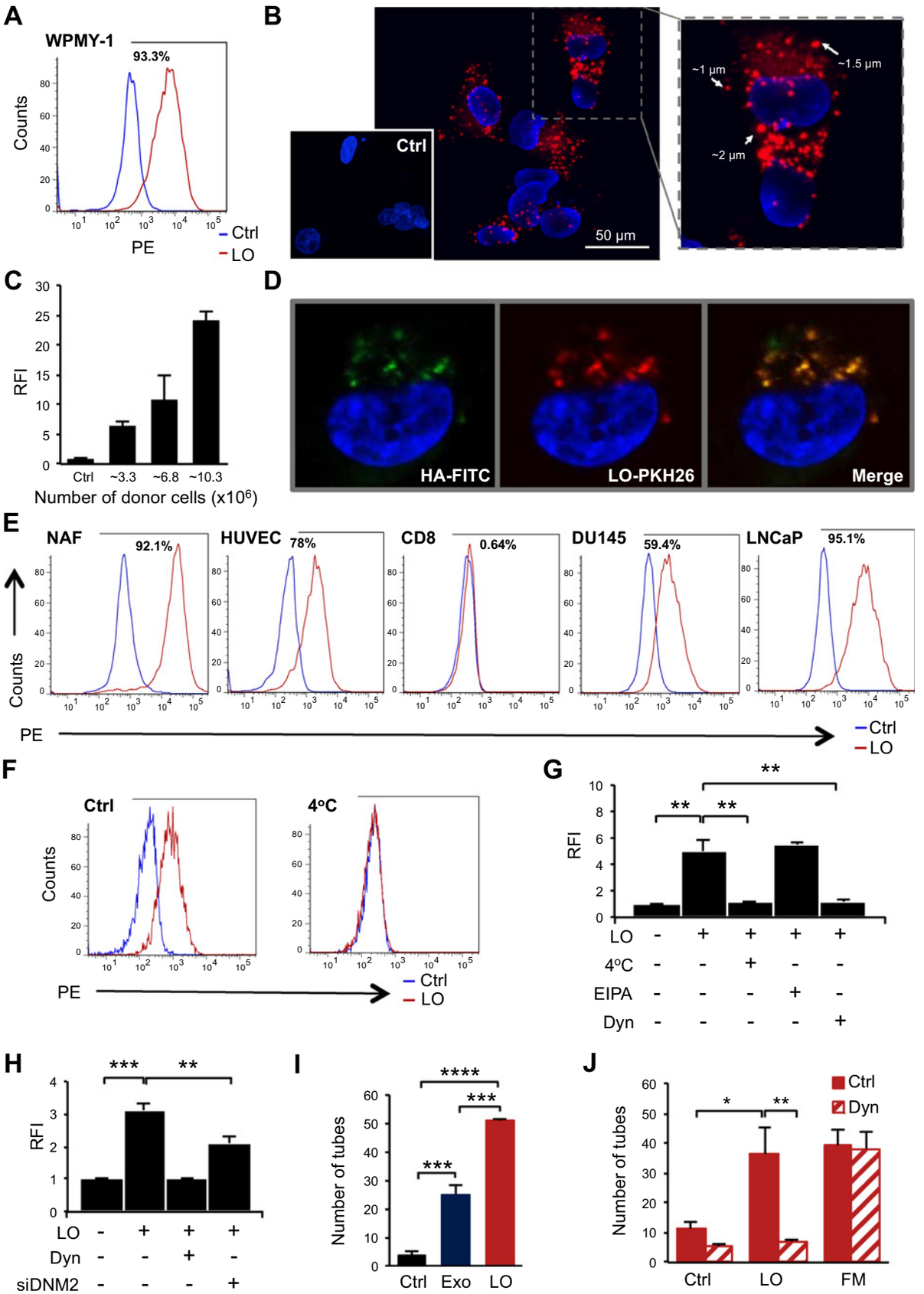

which is expressed in the donor cells but absent in the target cells. These results suggest that the particles were intact LO rather than empty circular membrane structures capturing the lipid dye. We then determined whether cells other than myofibroblasts could also internalize LO. We tested NAF, HUVEC, $CD8^+$ lymphocytes, and DU145 and LNCaP cancer cell lines. NAF are primary cells generated from prostatectomy tissues not associated with prostate cancer. LO uptake varied among these cells and was almost completely impaired in $CD8^+$ lymphocytes (Fig. 2E), implying a selective mechanism of uptake. These observations suggest that LO enter target cells by a mechanism that might involve defined interactions between LO and the recipient cells.

The biological effects of LO can be inhibited by blocking LO uptake

To further rule out the possibility that LO uptake occurs by a passive fusion of EV and cell membranes, we incubated target cells with LO at 4°C. This strategy has been previously used to inhibit ATP-dependent processes that are involved in EV endocytosis but not fusion (26). This approach efficiently prevented LO uptake (Fig. 2F), suggesting an active endocytic process. Due to their large size, we considered both phagocytosis and macropinocytosis as possible mechanisms. The PI3K inhibitor, Wortmannin (WTN), and the actin polymerization inhibitor, cytochalasin-D (CYT-D; refs. 27, 28), typically used to block both phagocytosis and macropinocytosis (29), significantly perturbed LO uptake (Supplementary Fig. S2B and S2C). To determine the relative contribution of these two processes, we used Dyn (30) and 5-(N-Ethyl-N-isopropyl) amiloride (EIPA), respectively. The primary and most ubiquitous target of Dyn is dynamin 2 (DNM2), which plays a role in the first stages of phagocytosis, including actin polymerization and augmenting of the membrane surface for particle engulfment (31, 32). EIPA, which inhibits the Na^+/H^+ antiporter (33), is typically used to block macropinocytosis. LO uptake was significantly inhibited by Dyn but not by EIPA (Fig. 2G; Supplementary Fig. S2D and S2E), suggesting that it occurs through a phagocytosis-like mechanism. The involvement of DNM2 in LO phagocytosis was further confirmed by a significant reduction in LO uptake upon specific silencing of DNM2 (Fig. 2H; Supplementary Fig. S2F). To determine whether the internalization is important for LO function, we employed tube formation assays, which have been previously used to show bioactivity of Exo (34) but have never been used to test LO function. Notably, LO stimulated a significant increase of the tube-branching abilities of HUVEC (Fig. 2I; Supplementary Fig. S2G). This effect was greater than that elicited by Exo and was obtained with amounts of LO (5–20 μg/mL) that are lower than those typically used for functional EV experiments (20–200 μg/mL; Supplementary Fig. S2H; refs. 6, 35). Dyn treatment of HUVEC cells prevented LO-induced tube branching, but did not prevent the branching induced by full media, which contains abundant soluble molecules that stimulate angiogenesis (Fig. 2J; Supplementary Fig. S2I). Collectively, these results indicate that LO enter the target cells through a phagocytosis-like mechanism, and that this is necessary for LO-mediated biological functions.

LO internalization induces a distinct fibroblast phenotype

Because it is known that tumor-activated fibroblasts release factors that can influence tube formation (36), and having observed a potent induction of tube branching in response to LO used directly to condition endothelial cells, we tested whether this effect in endothelial cells could be elicited by the secretions of fibroblasts that had internalized LO. CM from NAF pretreated with LO induced a more significant increase in tube branching than Exo (Fig. 3A; Supplementary Fig. S3A). To understand the molecular basis underlying the LO-induced result on NAF, we tested changes in expression of factors that are upregulated in fibroblasts activated by cancer cells (6, 14). LO treatment resulted in enhanced expression of IL6, matrix metalloproteinase 9 (MMP9; Fig. 3B), and α-smooth muscle actin (α-SMA; Fig. 3C). Conversely, TGFβ1, MMP1, and thrombospondin 1 (TSP1), which also have been recognized as markers of an activated, myofibroblast-like phenotype (6, 14, 36–38), were not altered (data not shown), suggesting that LO induce a distinct reprogramming of the fibroblasts, which results in a provascularization phenotype.

LO activate the TF MYC in NAF

TF activation might be an important mechanism underlying the responses of target cells to EVs (39). However, how frequently this happens and whether this phenomenon is specific for a given subpopulation of EVs, or for a given TF, has not yet been investigated. We thus tested if LO treatment perturbed TF activity, with the underlying hypothesis that this could be the mechanism modulating the effects described above. Nuclear extracts of fibroblasts exposed to LO or vehicle were tested for functional binding of TFs to DNA. We employed an activity array for TFs with a known role in somatic cell reprogramming (including EGR1, Nanog, SOX2, ETS, KLF4, MEF2, MYC, Pax6, TCF/LEF). Two independent trials revealed reproducible enhancement of MYC binding to DNA in response to LO (Supplementary Fig. S3B). To further validate this result, we measured MYC activity by examining the stimulation of MYC-dependent transcription. Significant activation of MYC-regulated CDK4 promoter was observed upon treatment with LO, but not with the same amount of Exo (Fig. 3D, $P < 0.05$). This estimation was based on protein concentration (20 μg/mL), normalized to the number of cells. However, we reasoned that the array was composed of very few TFs, and

Figure 2.

Internalization of LO in target cells is functionally important. **A,** WPMY-1 fibroblasts were exposed to PKH26-labeled LO from $LNCaP^{MyrAKT1}$ cells or vehicle for 1 hour. The shift of the red line to the right, which is quantifiable, indicates LO internalization by the target cells, and it is expressed as percentage of cells internalizing LO. **B,** Cells negative and positive for PKH26 were FACS-sorted and imaged by confocal microscopy demonstrating the presence of abundant vesicular structures in the LO size range. Control cells are visible in the bottom left plot. **C,** WPMY-1 cells were incubated with increasing doses of PKH26-labeled LO and then analyzed by FACS. Uptake rates, expressed as RFI, correlate with LO doses. **D,** PKH26-positive WPMY-1 cells were sorted and stained with a HA-FITC antibody against the HA-tag on the MyrAKT1 construct. The two signals colocalize in internalized EVs. **E,** FACS analysis demonstrates variable uptake rate in the indicated cell lines exposed to PKH26-labeled LO. **F,** Treatment of WPMY-1 cells with LO at 4°C inhibits the uptake. **G,** LO uptake by WPMY-1 cells was significantly inhibited by Dyn (20 μmol/L) but not by EIPA (50 μmol/L). As expected, uptake was inhibited at 4°C. **H,** Transient silencing of DNM2 (siDNM2) in WPMY-1 cells resulted in a significant reduction of LO uptake. **I,** HUVEC were seeded on Matrigel-coated wells and exposed to Exo or LO (20 μg/mL). The number of branched tubes was significantly altered by both LO and Exo. **J,** Dyn treatment prevented the LO-induced tube formation. Bar plots show the average of three biological replicates (*, $P < 0.05$; **, $P < 0.02$; ***, $P < 0.002$; and ****, $P < 0.000001$).

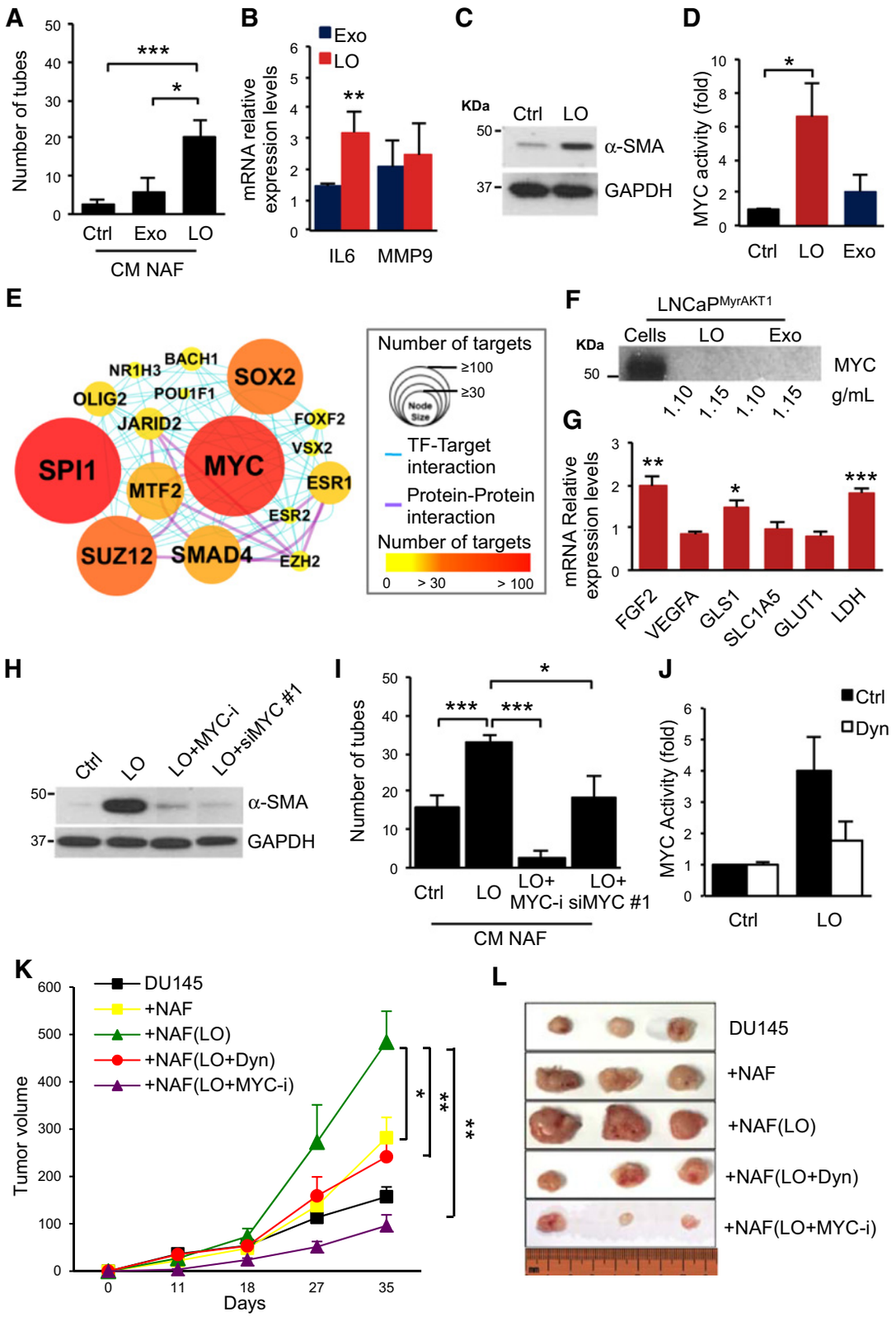

a large-scale approach might be useful to unambiguously define the TF pathways involved in LO-mediated activation. RNA-seq was carried out in NAF exposed to LO or vehicle to obtain an in-depth analysis of the transcriptome of these cells in response to LO. This analysis, performed in biological duplicate, identified 207 differentially expressed genes (DEG; FDR < 0.1, fold change $\geq$ 1.5) in response to LO. MRA was then applied to the DEG set using TF-target interaction information collected from public databases. This allowed us to infer functional interactions between TFs and their target genes following a strategy we previously employed to identify important transcriptional regulators (21). Sixteen of a total of 274 activated TFs emerged as strong putative TFs (empirical test P value < 0.01 and hypergeometric test P value < 0.01). The number of putative TFs that were activated by LO is relatively small (~6%), suggesting that modulation of gene expression is selective. MYC emerged as a highly activated TF in response to LO (Fig. 3E; Supplementary Table S2), confirming our initial results. MYC was not identified in LO, suggesting that LO stimulate MYC activation rather than mediating transfer of the protein (Fig. 3F). Detection of higher levels of MYC in cancer-associated fibroblasts compared with NAF (Supplementary Fig. S3C) supports the concept that this activation might occur naturally in the tumor microenvironment. Furthermore, NAF exposed to LO exhibited increased levels of fibroblast growth factor 2 (FGF2), glutaminase (GLS), and lactate dehydrogenase (LDH), which are known transcriptional targets of MYC (Fig. 3G). Notably, human RNA expression data demonstrated that LDH positively correlates with MYC in prostate cancer tissues with high stromal content (> 70%; Supplementary Fig. S3D). These results support an LO-dependent modulation of MYC activity in fibroblasts.

LO-induced NAF activation is mediated by MYC

The above results prompted us to test whether MYC plays a functional role in LO-mediated fibroblast reprogramming. Both genetic silencing of MYC using MYC inhibition by the low molecular weight compound 10058-F4 (40) and two independent siRNAs (Supplementary Fig. S3E) in NAF were sufficient to block the LO-induced α-SMA increase and the ability of these cells to stimulate branching morphogenesis (Fig. 3H and I; Supplementary Fig. S3F–S3I). The LO-induced MYC activity was blocked by the MYC inhibitor confirming the specific effect of the compound (Supplementary Fig. S3J). A tumor supportive role for stromal MYC was also independently demonstrated by animal experiments in which overexpression of MYC in wild-type mouse primary prostatic fibroblasts induced hyperplasia of the adjacent normal prostatic epithelium in tissue recombinants grafted into the subrenal capsule of syngeneic C57BL/6 mice (Supplementary Fig. S3K). Interestingly, the LO-induced MYC activation was reduced in NAF by blocking LO uptake with Dyn (Fig. 3J), further confirming the effect of this compound on tube branching described above (Fig. 2J). To investigate the contribution of LO–stroma interactions *in vivo*, DU145 cells, alone or recombined with NAF, were injected subcutaneously in nude mice, and tumor growth was measured for up to 35 days. Recombination of tumor cells with NAF led to an approximately 1.5-fold increase of the mean tumor volume compared with the tumor cells alone. Notably, *ex vivo* pretreatment of NAF for 3 days with LO isolated from LNCaP^{MyrAKT1} significantly enhanced tumor growth (~3-fold higher than tumor cells alone). This effect was completely prevented by blocking LO uptake with Dyn and reduced by treatment with the MYC inhibitor (Fig. 3K and L). Treatment with the MYC inhibitor alone also prevented the NAF-supported tumor growth (data not shown). Together, these data provide evidence of an important functional role for MYC in fibroblast reprogramming and modulation of tumor growth mediated by AKT1-loaded LO.

MYC activation in the stroma is dependent on AKT1 kinase activity

Because most of the results described so far were elicited by LO originating from cells expressing a constitutively active AKT1, and because we found high levels of p-AKT1^{Ser473} in LO, we wondered whether this kinase was functionally active in the particles. We first demonstrated that MyrAKT1 can be readily immunoprecipitated in LO (Supplementary Fig. S4A). Then, the AKT1 immunoprecipitation products from the two EV populations, cultured in cell- and serum-free culture conditions for up to 72 hours, were submitted to a AKT1 kinase activity assay, which demonstrated abundant phosphorylation of the AKT1 target glycogen synthase kinase 3α/β (GSK3α/β) in LO, but not in Exo (Fig. 4A). In support of the hypothesis that LO might function as mobile platforms for active kinase, LO induced upregulation of p-AKT1^{Ser473} in NAF (Fig. 4B; Supplementary Fig. S4B). We then tested whether AKT1 activity is necessary for the LO-mediated effects on the stroma. MYC activity (Fig. 4C), α-SMA levels (Fig. 4D), and tube branching (Fig. 4E; Supplementary Fig. S4C and S4D) were reduced in NAF exposed to LO in the presence of the AKT1 inhibitor AZD5363 (41) in comparison with vehicle treatment. The result on tube branching was reproduced with LO derived from an unrelated prostate cancer cell line that endogenously expresses an active AKT1 (Fig. 4E). Collectively, these data suggest that the

Figure 3.

LO treatment of NAF induces a MYC-dependent reprogramming. **A,** HUVEC cells were exposed to CM from NAF, previously incubated with LO and Exo. The CM from NAF pretreated with LO, but not Exo, induced tube formation. **B,** qRT-PCR of NAF exposed to LO or vehicle shows increased levels of IL6 and MMP9 mRNA in response to LO treatment. **C,** Immunoblot experiments demonstrated increased levels of α-SMA in NAF upon 24-hour exposure to LO. **D,** Luciferase activity of MYC-regulated CDK4 promoter significantly increased in NAF exposed to LO but not Exo. **E,** MRA of DEG obtained after RNA-seq in NAF treated with LO or vehicle. MYC is one of the most active TF in NAF in response to LO. TF network illustrating interactions between key TFs and the degree of influence to potential target genes among the DEGs (node size and color, respectively). TFs with a large number of targets (> 105) are represented by big red nodes, whereas TFs with smaller numbers of targets (< 50) are indicated with small yellow nodes. Cyan and purple connectors indicate TF–target and protein–protein interactions, respectively. **F,** Protein lysate from LNCaP^{MyrAKT1} cells and derived LO and Exo were blotted with MYC antibody. **G,** qRT-PCR in NAF, exposed to LO or vehicle, shows increase levels of MYC targets in response to LO. **H,** Immunoblot analysis showing that MYC inhibition, using either the MYC inhibitor 10058F4 (MYC-i; 20 μmol/L) or siRNA specific for MYC (siMYC), prevents LO-dependent induction of α-SMA. **I,** HUVEC cells were exposed to CM from NAF previously incubated with LO with or without MYC inhibition. MYC inhibition (MYC-i, siMYC) induces a reduction of tube formation in response to LO. **J,** Luciferase activity of the MYC-regulated promoter in response to LO is inhibited by Dyn. **K,** DU145 cells were injected subcutaneously into nude mice with or without NAF (ratio 4:1) and the tumor volume (mean ± SE) measured at the indicated intervals (tumors $n \geq 5$ per group). The NAF were either untreated or exposed, *ex vivo*, to LO in the presence or absence of Dyn or MYCi for 72 hours. LO treatment increased significantly the tumor volume, an effect inhibited by both Dyn and MYC-i. **L,** Representative gross photographs of the tumors. Plots shows the average of three biological replicate (*, $P < 0.05$; **, $P < 0.02$; ***, $P < 0.002$).

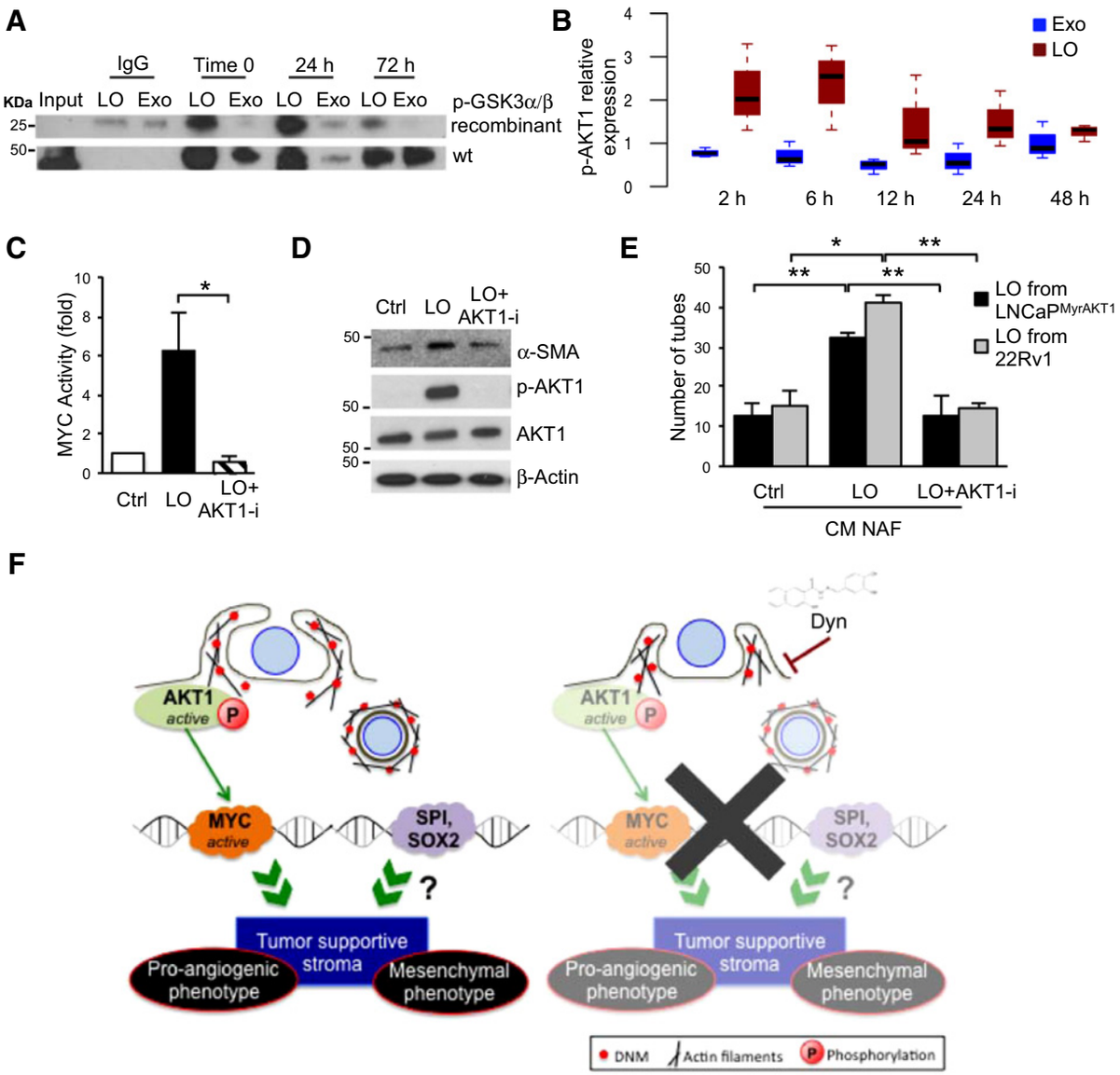

Figure 4.

LO-induced NAF reprogramming is mediated by AKT1 activation. **A,** Protein lysates from LO or Exo were used to immunoprecipitate MyrAKT1 using an HA antibody and IP product subjected to AKT1 kinase activity assay using GSK3α/β-recombinant protein as a substrate. Both the IP product and the input (straight protein lysates) were then blotted with a p-GSK3α/β$^{Ser21/9}$ antibody, which recognizes the wild-type (wt) protein as well as the recombinant protein, demonstrating the presence of active AKT1 in LO but not in Exo. **B,** NAF exposed to LO or Exo for the indicated times were immunoblotted with p-AKT1^{Ser473} and AKT1 antibodies. The box plot shows the average of the p-AKT1^{Ser473} band intensity, normalized over β-actin, from three different experiments. **C,** Luciferase activity of the MYC-regulated promoter in response to LO inhibited by the AKT1 inhibitor AZD5363 (AKT1-i; 1 μmol/L). Bar plot shows the average of three biological replicates (*, $P < 0.05$). **D,** Immunoblot assay showing that AKT1 inhibition prevents LO-dependent induction of α-SMA. **E,** Tube branching in response to LO is reduced by AKT1-i. Bar plots show the average of three biological replicates (*, $P < 0.05$; **, $P < 0.02$). **F,** Our working model suggests that AKT1, which is activated upon LO treatment, can phosphorylate, thus inactivating it, the MYC inhibitor GSK3α/β. Active MYC induces a reprogramming of NAF characterized by upregulation of α-SMA, LDH, and FGF2, and this process can be inhibited by preventing LO internalization.

LO-induced fibroblast reprogramming is dependent on AKT1 kinase activity.

Discussion

In this study, we demonstrate that AKT1 is a LO-resident protein that maintains its activity inside these vesicles and can be detected in LO isolated from plasma of patients with metastatic prostate cancer. This result supports the novel observation that EVs are a heterogeneous category of particles (11, 42). This might be clinically significant because it implies that different EV populations can harbor distinct molecules that can be interrogated as biomarkers.

Although previous studies on Exo have identified TGFβ1 as a key player in modulating the response of the stroma (6, 35), LO

treatment of fibroblasts promotes MYC-dependent reprogramming characterized by upregulation of molecules involved in stroma activation, angiogenesis, and metabolism, and prevented by inhibiting LO internalization and/or AKT1 activity. While the effect of EVs on the endothelium has been previously revealed (3, 4), our study shows an alternative mechanism that alters the endothelium indirectly by activating fibroblasts. This might be an effect not targetable by angiogenesis inhibitors and could be used to develop therapeutic strategies alternative or complementary to antiangiogenesis strategies. LO can condition the fibroblasts promoting their tumor-supportive functions *in vivo*, and this result is abolished not only by MYC inhibition but also by preventing LO uptake with Dyn. A critical feature of LO-mediated reprogramming is therefore the activation of MYC, and we speculate that this might promote fibroblast responses at different levels. LO-mediated MYC activation could be responsible for the acquired ability of the fibroblasts to induce tube formation by regulating its downstream target FGF2 (43). It could also contribute to tumor progression by altering the metabolism of the target fibroblasts as suggested by the observed GLS and LDH upregulation in response to LO, and the significant correlation between MYC and LDH in the tumor stroma *in vivo*. This is important because it could explain, at least in part, the metabolic switch described in tumor-associated fibroblasts (44). Although MYC is a known transcriptional enhancer of genes involved in glycolysis and glutaminolysis often observed in metastatic tumors (45), the demonstration that this might happen in the stroma, and as a response to a discrete EV population that is tumor-specific, is completely novel.

These results strongly point to MYC as one of the master regulators of LO-induced activities in the stroma. Two independent large-scale approaches (TF activity array and RNA-Seq) further suggest that LO might play a more complex function in regulating the response of the fibroblasts to the tumor. We have evidence for additional TFs, with several common targets, whose function is activated by LO. One example is the ETS family member SPI-1 (Fig. 3E), which is known for its role in orchestrating cell fate in hematopoiesis but has been poorly studied in cancer (46) and not at all in the stroma. This TF seems to be highly sensitive to LO regulation, as inferred by the result that it controls most of the DEGs in response to LO. It also shares 125 target genes with MYC (Supplementary Fig. S4E), suggesting that it might cooperate with MYC in regulating gene expression changes in response to LO. A functional array demonstrated that a class of TFs that recognized an ETS binding domain was highly activated in response to LO (Supplementary Fig. S3B). Notably, the ETS TF family has been previously shown to mediate reprogramming of breast cancer–associated fibroblasts in response to PTEN loss (47). Another example is represented by SOX2, which is also robustly activated in response to LO (Fig. 3E; Supplementary Fig. S3B), and has been previously shown to induce properties of mesenchymal stem cells when overexpressed in fibroblasts (48). These considerations led us to a working model in which LO uptake by fibroblasts results in activation of AKT1 and possibly other signaling pathways, which in turn affect transcriptional programs that are regulated by reprogramming factors such as MYC, SPI-1, ETS, and SOX2. These TFs could thus all contribute to reprogram the stroma in favor of a tumor-supportive phenotype (Fig. 4F).

Our observation that inhibition of AKT1 in the fibroblasts abolishes the LO-induced alterations to a degree that is similar to that provoked by inhibition of LO uptake allows us to speculate that preventing phagocytosis of these large vesicles might be a more global strategy to prevent communication between cells and stromal cells than targeting single molecules. To our knowledge, this result has not been previously demonstrated for other EVs. This has important implications, considering that EVs harbor a variety of molecules and blocking the uptake of the whole vesicle instead of inhibiting one or two specific molecules might be a more efficient strategy to prevent dissemination of oncogenic signals (49). This could be combined with current therapies aimed to target tumor cells but not the tumor-supportive environment. In addition, inhibition of EV uptake could block the effect of circulating EVs that are not eliminated with surgery excision or radiation-induced ablation and thus the combined approach might prevent or delay the tumor relapse. However, a deeper understanding of the molecular basis underlying LO phagocytosis is necessary to develop therapeutic strategies aimed to block EV interactions with target cells. For example, it will be important to know whether the activation of AKT1, observed in this study, is the result of endomembrane release of the LO cargo upon fusion of LO membranes with the surrounding endosomes, or if the endogenous protein is recruited and activated by ligand-receptor–induced signaling in response to LO.

In conclusion, this is the first study demonstrating the role of LO in educating the fibroblasts to a tumor-supportive function. We identified a novel AKT1/MYC signaling axis that originates from the tumor and reverberates to the stroma as a specific mediator of LO biological effects. However, the complexity of LO cargo and the resulting molecular effects elicited in target cells suggest that other players contribute to the phenotypic changes elicited by LO. Additional studies will further elucidate the function of LO in the modulation of the tumor microenvironment and identify additional nodes that could be targeted to prevent tumor progression and metastasis.

Disclosure of Potential Conflicts of Interest

N.A. Bhowmick is a researcher at Veterans Administration Greater Los Angeles Healthcare System. No potential conflicts of interest were disclosed by the other authors.

Authors' Contributions

Conception and design: V.R. Minciacchi, D. Di Vizio
Development of methodology: V.R. Minciacchi, C. Spinelli, M. Reis-Sobreiro, L. Cavallini, M. Zandian, P. Chiarugi, E. Cocucci, X. Li, R. Mishra
Acquisition of data (provided animals, acquired and managed patients, provided facilities, etc.): N.A. Bhowmick, E.M. Posadas, P. Chiarugi, G. Viglietto, E. Cocucci
Analysis and interpretation of data (e.g., statistical analysis, biostatistics, computational analysis): S. You, V.R. Minciacchi, R.M. Adam, M.R. Freeman, D. Di Vizio
Writing, review, and/or revision of the manuscript: V.R. Minciacchi, M.R. Freeman, E. Cocucci, D. Di Vizio
Administrative, technical, or material support (i.e., reporting or organizing data, constructing databases): P. Chiarugi, E.M. Posadas
Study supervision: D. Di Vizio

Acknowledgments

We would like to thank first of all our patients and their families for participation in this study. We are grateful to Drs. Chia-Yi Chu and Wen-Chin Huang for their technical support for the animal experiment, to Izon Science (Subhash Kalluri) for the TRPS, to Drs. Andries Zijlstra, Francesca Demichelis,

and Amina Zoubedi for constructive comments, and to Dr. Dennis Hazelett for using his pipeline for normalization of the RNA-seq data.

Grant Support

This study was supported by grants from the NIH (NIH UCLA SPORE in Prostate Cancer award P50 CA092131 to D. Di Vizio); Avon Breast Cancer Foundation Fund 02-2013-043 to D. Di Vizio; the Martz Translational Breast Cancer Research Fund to M.R. Freeman and D. Di Vizio; Department of Defense PC150836 to D. Di Vizio; the Steven Spielberg Discovery Fund in Prostate Cancer Research to M.R. Freeman and D. Di Vizio; and The Ohio State University Comprehensive Cancer Center (P30-CA016058) and an intramural fund (IRP46050-502339) to E. Cocucci.

The costs of publication of this article were defrayed in part by the payment of page charges. This article must therefore be hereby marked *advertisement* in accordance with 18 U.S.C. Section 1734 solely to indicate this fact.

Received November 1, 2016; revised December 12, 2016; accepted February 2, 2017; published OnlineFirst February 15, 2017.

References

1. Barron DA, Rowley DR. The reactive stroma microenvironment and prostate cancer progression. Endocr Relat Cancer 2012;19:R187–204.
2. Tripathi M, Billet S, Bhowmick NA. Understanding the role of stromal fibroblasts in cancer progression. Cell Adh Migr 2012;6:231–5.
3. Al-Nedawi K, Meehan B, Micallef J, Lhotak V, May L, Guha A, et al. Intercellular transfer of the oncogenic receptor EGFRvIII by microvesicles derived from tumour cells. Nat Cell Biol 2008;10:619–24.
4. Minciacchi VR, Freeman MR, Di Vizio D. Extracellular vesicles in cancer: Exosomes, microvesicles and the emerging role of large oncosomes. Semin Cell Dev Biol 2015;40:41–51.
5. Peinado H, Aleckovic M, Lavotshkin S, Matei I, Costa-Silva B, Moreno-Bueno G, et al. Melanoma exosomes educate bone marrow progenitor cells toward a pro-metastatic phenotype through MET. Nat Med 2012;18: 883–91.
6. Webber JP, Spary LK, Sanders AJ, Chowdhury R, Jiang WG, Steadman R, et al. Differentiation of tumour-promoting stromal myofibroblasts by cancer exosomes. Oncogene 2015;34:290–302.
7. Di Vizio D, Kim J, Hager MH, Morello M, Yang W, Lafargue CJ, et al. Oncosome formation in prostate cancer: association with a region of frequent chromosomal deletion in metastatic disease. Cancer Res 2009; 69:5601–9.
8. Meehan B, Rak J, Di Vizio D. Oncosomes - large and small: What are they, where they came from? J Extracell Vesicles 2016;5:33109.
9. Hager MH, Morley S, Bielenberg DR, Gao S, Morello M, Holcomb IN, et al. DIAPH3 governs the cellular transition to the amoeboid tumour phenotype. EMBO Mol Med 2012;4:743–60.
10. Di Vizio D, Morello M, Dudley AC, Schow PW, Adam RM, Morley S, et al. Large oncosomes in human prostate cancer tissues and in the circulation of mice with metastatic disease. Am J Pathol 2012;181:1573–84.
11. Minciacchi VR, You S, Spinelli C, Morley S, Zandian M, Aspuria PJ, et al. Large oncosomes contain distinct protein cargo and represent a separate functional class of tumor-derived extracellular vesicles. Oncotarget 2015; 6:11327–41.
12. Morello M, Minciacchi VR, de Candia P, Yang J, Posadas E, Kim H, et al. Large oncosomes mediate intercellular transfer of functional microRNA. Cell Cycle 2013;12:3526–36.
13. Adam RM, Mukhopadhyay NK, Kim J, Di Vizio D, Cinar B, Boucher K, et al. Cholesterol sensitivity of endogenous and myristoylated Akt. Cancer Res 2007;67:6238–46.
14. Giannoni E, Bianchini F, Masieri L, Serni S, Torre E, Calorini L, et al. Reciprocal activation of prostate cancer cells and cancer-associated fibroblasts stimulates epithelial-mesenchymal transition and cancer stemness. Cancer Res 2010;70:6945–56.
15. Osteikoetxea X, Balogh A, Szabo-Taylor K, Nemeth A, Szabo TG, Paloczi K, et al. Improved characterization of EV preparations based on protein to lipid ratio and lipid properties. PLoS One 2015;10:e0121184.
16. Cocucci E, Gaudin R, Kirchhausen T. Dynamin recruitment and membrane scission at the neck of a clathrin-coated pit. Mol Biol Cell 2014;25: 3595–609.
17. Taddei ML, Cavallini L, Comito G, Giannoni E, Folini M, Marini A, et al. Senescent stroma promotes prostate cancer progression: The role of miR-210. Mol Oncol 2014;8:1729–46.
18. Hermeking H, Rago C, Schuhmacher M, Li Q, Barrett JF, Obaya AJ, et al. Identification of CDK4 as a target of c-MYC. Proc Natl Acad Sci U S A 2000;97:2229–34.
19. Langmead B, Trapnell C, Pop M, Salzberg SL. Ultrafast and memory-efficient alignment of short DNA sequences to the human genome. Genome Biol 2009;10:R25.
20. Li B, Dewey CN. RSEM: Accurate transcript quantification from RNA-Seq data with or without a reference genome. BMC Bioinformatics 2011;12:323.
21. Yang W, Ramachandran A, You S, Jeong H, Morley S, Mulone MD, et al. Integration of proteomic and transcriptomic profiles identifies a novel PDGF-MYC network in human smooth muscle cells. Cell Commun Signal 2014;12:44.
22. Cheng N, Bhowmick NA, Chytil A, Gorksa AE, Brown KA, Muraoka R, et al. Loss of TGF-beta type II receptor in fibroblasts promotes mammary carcinoma growth and invasion through upregulation of TGF-alpha-, MSP- and HGF-mediated signaling networks. Oncogene 2005;24:5053–68.
23. Di Vizio D, Demichelis F, Simonetti S, Pettinato G, Terracciano L, Tornillo L, et al. Skp2 expression is associated with high risk and elevated Ki67 expression in gastrointestinal stromal tumours. BMC Cancer 2008;8:134.
24. van der Mijn JC, Sol N, Mellema W, Jimenez CR, Piersma SR, Dekker H, et al. Analysis of AKT and ERK1/2 protein kinases in extracellular vesicles isolated from blood of patients with cancer. J Extracell Vesicles 2014;3:25657.
25. Abels ER, Breakefield XO. Introduction to Extracellular vesicles: Biogenesis, RNA cargo selection, content, release, and uptake. Cell Mol Neurobiol 2016;36:301–12.
26. Svensson KJ, Christianson HC, Wittrup A, Bourseau-Guilmain E, Lindqvist E, Svensson LM, et al. Exosome uptake depends on ERK1/2-heat shock protein 27 signaling and lipid Raft-mediated endocytosis negatively regulated by caveolin-1. J Biol Chem 2013;288:17713–24.
27. Araki N, Johnson MT, Swanson JA. A role for phosphoinositide 3-kinase in the completion of macropinocytosis and phagocytosis by macrophages. J Cell Biol 1996;135:1249–60.
28. Swanson JA. Shaping cups into phagosomes and macropinosomes. Nat Rev Mol Cell Biol 2008;9:639–49.
29. Falcone S, Cocucci E, Podini P, Kirchhausen T, Clementi E, Meldolesi J. Macropinocytosis: Regulated coordination of endocytic and exocytic membrane traffic events. J Cell Sci 2006;119:4758–69.
30. Macia E, Ehrlich M, Massol R, Boucrot E, Brunner C, Kirchhausen T. Dynasore, a cell-permeable inhibitor of dynamin. Dev Cell 2006;10: 839–50.
31. Kinchen JM, Doukoumetzidis K, Almendinger J, Stergiou L, Tosello-Trampont A, Sifri CD, et al. A pathway for phagosome maturation during engulfment of apoptotic cells. Nat Cell Biol 2008;10:556–66.
32. Kinchen JM, Ravichandran KS. Phagosome maturation: Going through the acid test. Nat Rev Mol Cell Biol 2008;9:781–95.
33. Commisso C, Davidson SM, Soydaner-Azeloglu RG, Parker SJ, Kamphorst JJ, Hackett S, et al. Macropinocytosis of protein is an amino acid supply route in Ras-transformed cells. Nature 2013;497:633–7.
34. Kosaka N, Iguchi H, Yoshioka Y, Takeshita F, Matsuki Y, Ochiya T. Secretory mechanisms and intercellular transfer of microRNAs in living cells. J Biol Chem 2010;285:17442–52.
35. Webber J, Steadman R, Mason MD, Tabi Z, Clayton A. Cancer exosomes trigger fibroblast to myofibroblast differentiation. Cancer Res 2010;70: 9621–30.
36. Orimo A, Gupta PB, Sgroi DC, Arenzana-Seisdedos F, Delaunay T, Naeem R, et al. Stromal fibroblasts present in invasive human breast carcinomas promote tumor growth and angiogenesis through elevated SDF-1/CXCL12 secretion. Cell 2005;121:335–48.
37. Kalluri R, Zeisberg M. Fibroblasts in cancer. Nat Rev Cancer 2006;6: 392–401.
38. Serini G, Gabbiani G. Mechanisms of myofibroblast activity and phenotypic modulation. Exp Cell Res 1999;250:273–83.

39. Cossetti C, Iraci N, Mercer TR, Leonardi T, Alpi E, Drago D, et al. Extracellular vesicles from neural stem cells transfer IFN-gamma via Ifngr1 to activate Stat1 signaling in target cells. Mol Cell 2014;56: 193–204.
40. Yin X, Giap C, Lazo JS, Prochownik EV. Low molecular weight inhibitors of Myc-Max interaction and function. Oncogene 2003;22:6151–9.
41. Lamoureux F, Thomas C, Crafter C, Kumano M, Zhang F, Davies BR, et al. Blocked autophagy using lysosomotropic agents sensitizes resistant prostate tumor cells to the novel Akt inhibitor AZD5363. Clin Cancer Res 2013;19:833–44.
42. Kowal J, Arras G, Colombo M, Jouve M, Morath JP, Primdal-Bengtson B, et al. Proteomic comparison defines novel markers to characterize heterogeneous populations of extracellular vesicle subtypes. Proc Natl Acad Sci U S A 2016;113:E968–77.
43. Xue G, Yan HL, Zhang Y, Hao LQ, Zhu XT, Mei Q, et al. c-Myc-mediated repression of miR-15–16 in hypoxia is induced by increased HIF-2alpha and promotes tumor angiogenesis and metastasis by upregulating FGF2. Oncogene 2015;34:1393–406.
44. Pavlides S, Whitaker-Menezes D, Castello-Cros R, Flomenberg N, Witkiewicz AK, Frank PG, et al. The reverse Warburg effect: Aerobic glycolysis in cancer associated fibroblasts and the tumor stroma. Cell Cycle 2009; 8:3984–4001.
45. Dang CV. MYC on the path to cancer. Cell 2012;149:22–35.
46. Yu M, Al-Dallal S, Al-Haj L, Panjwani S, McCartney AS, Edwards SM, et al. Transcriptional regulation of the proto-oncogene Zfp521 by SPI1 (PU.1) and HOXC13. Genesis 2016;54:519–33.
47. Bronisz A, Godlewski J, Wallace JA, Merchant AS, Nowicki MO, Mathsyaraja H, et al. Reprogramming of the tumour microenvironment by stromal PTEN-regulated miR-320. Nat Cell Biol 2011;14:159–67.
48. Szabo P, Kolar M, Dvorankova B, Lacina L, Stork J, Vlcek C, et al. Mouse 3T3 fibroblasts under the influence of fibroblasts isolated from stroma of human basal cell carcinoma acquire properties of multipotent stem cells. Biol Cell 2011;103:233–48.
49. Sung BH, Ketova T, Hoshino D, Zijlstra A, Weaver AM. Directional cell movement through tissues is controlled by exosome secretion. Nat Commun 2015;6:7164.